Available online at www.sciencedirect.com
SCIENCE DIRECT®
International Journal of Multiphase Flow 32 (2006) 807–822
International Journal of Multiphase Flow
www.elsevier.com/locate/ijmulflow

Breakup and atomization characteristics of mono-dispersed diesel droplets in a cross-flow air stream

Sung Wook Park [a], Sayop Kim [b], Chang Sik Lee [c,*]

[a] Mechanical Engineering and Technical Research Institute, Hanyang University, 17 Haengdang-dong, Sungdong-gu, Seoul 133-791, South Korea
[b] Graduate School of Hanyang University, 17 Haengdang-dong, Sungdong-gu, Seoul 133-791, South Korea
[c] Department of Mechanical Engineering, Hanyang University, 17 Haengdang-dong, Sungdong-gu, Seoul 133-791, South Korea

Received 1 February 2006; received in revised form 23 February 2006

Abstract

This paper describes the microscopic and macroscopic breakup characteristics, as well as the velocity and size distributions, of mono-dispersed droplets in relation to the breakup regimes. For this experiment, a droplet generator equipped with a piezo stack produced mono-dispersed droplets. The droplet-breakup phenomenon due to the cross-flow was captured in microscopic and macroscopic views by using the following: a spark lamp, a Nd:YAG laser, a long distance microscope and a CCD camera as a function of the Weber number. Along with the analysis of the images, the droplet size and velocity distributions were measured in the near nozzle region by a phase Doppler particle analyzer system at bag, stretching and thinning, and catastrophic breakup regimes. The results of this study showed the size and velocity distributions of disintegrated droplets at the bag, stretching and thinning, and catastrophic breakup regimes. In the bag breakup regime, the droplets separated into small and large droplets during breakup. Alternatively, the droplets disintegrated at a shorter duration and formed a cloud, similar to a fuel spray injected through an injector, in the stretching and thinning and catastrophic breakup regimes.

Keywords: Breakup mechanism; Mono-dispersed droplets; SMD (Sauter mean diameter); PDPA (phase Doppler particle analyzer)

1. Introduction

In an internal combustion engine, the atomization of fuel spray is important because of its close relation to the engine efficiency and pollutant emissions. In particular, in the case of a diesel engine, the atomization of the fuel spray is very important because there is little atomization for diesel as compared to gasoline spray. In order to improve the atomization performance of a diesel spray, there have been many attempts for the better

* Corresponding author. Tel.: +82 2 2220 0427; fax: +82 2 2281 5286.
E-mail address: cslee@hanyang.ac.kr (C.S. Lee).

0301-9322/$ - see front matter © 2006 Elsevier Ltd. All rights reserved.
doi:10.1016/j.ijmultiphaseflow.2006.02.019

atomization of the fuel spray. For example, application of an electronic control common-rail system causes the injection pressure to become higher. There are several studies on the effect of injection pressure on the atomization characteristics. Lee and Park (2002), Park et al. (2003), Hountalas et al. (2004) and Lee et al. (2005) showed that the spray atomization performance is dependent on the injection. Additionally, in order to produce well-atomized fuel sprays, Payri et al. (2004) and Baik et al. (2003) investigate the optimization of nozzle.

Along with the atomization characteristics of diesel fuel sprays, Liu and Reitz (1997) performed fundamental studies on diesel droplet-breakup phenomena in order to uncover the breakup mechanism of a diesel droplet. An investigation on the distortion and breakup mechanisms of liquid drops injected into a traversed high velocity air jet reveal the transitions of droplet-breakup mechanisms and the characteristics of droplet distortion. Lee and Reitz (2001) studied the breakup mechanisms of liquid drops in high-velocity airflows and compared the breakup mechanisms between water and diesel droplets. In addition, there are many other studies on liquid droplet breakup investigated by Krzeczkowski (1980), Hwang et al. (1996) and Hsiang and Faeth (1992).

Previous studies concerning droplet-breakup mechanisms focus on the analysis of high-magnification photography using a spark lamp and a long distance microscope. The microscopic image, that is, those obtained using a long distance microscope, are good for investigating the breakup mechanisms. However, considering that the final goal of studies on droplet breakup is to control the droplet breakup characteristics, the distributions of droplet size and velocity after breakup are important results. There are various kinds of apparatuses to measure the droplet size distribution, such as the widely used image processing for particle sizing showed by Kim and Lee (2002) and Koh et al. (2001). However, this method is limited in the droplet density because of the difficulty in processing overlapped droplets. The measurements of size and velocity distributions based on the Doppler signal can also be helpful for analyzing the atomization characteristics of droplets. Many researchers such as Lee and Reitz (2004), Park and Lee (2003) and Schunemann et al. (1998) use the PDPA (phase Doppler particle analyzer) system to characterize the atomization characteristics of fuel liquid; therefore, it has been regarded as an appropriate apparatus. Consequently, the PDPA measurement results for the droplet-breakup region can provide better understanding on the droplet disintegration mechanism.

One goal of this study was to visualize the breakup process of mono-dispersed droplets in macroscopic and microscopic views. Another goal of this study was to obtain size and velocity distributions of disintegrated droplets in the following breakup regimes: bag, stretching and thinning, and catastrophic. A droplet generator with a piezo stack was used to produce the mono-dispersed droplets. The size and velocity of the produced droplets were measured using the PDPA system in accordance to the frequency applied to the piezo stack.

2. Experimental apparatus and procedure

2.1. Experimental apparatus

2.1.1. Droplet generator, gas nozzle and droplet visualization system

As shown in Fig. 1, mono-dispersed droplets with same droplet size and velocity are produced by the droplet generator and injected into a gas stream ejected from gas nozzle. The droplet generator was composed of a nozzle and a vibrating piezo stack. When the liquid passed through the nozzle, the vibrating piezo stack cut the liquid jet to generate droplets. Therefore, the frequency applied to the piezo stack was important for producing uniform droplets.

In this experiment, the droplet generator had a 100-μm orifice nozzle and the optimal frequency (f_{opt}) applied to the vibrating piezo stack of the droplet generator was determined using

$$f_{opt} = 0.282\frac{\dot{Q}}{D_n^3}, \tag{1}$$

where $\dot{Q}$ is the volumetric flow rate and D_n is the diameter of the nozzle orifice. Additionally, a function generator and voltage amplifier generated a square wave signal with a peak-to-peak voltage of 30 V, which operated the piezoelectric droplet generator.

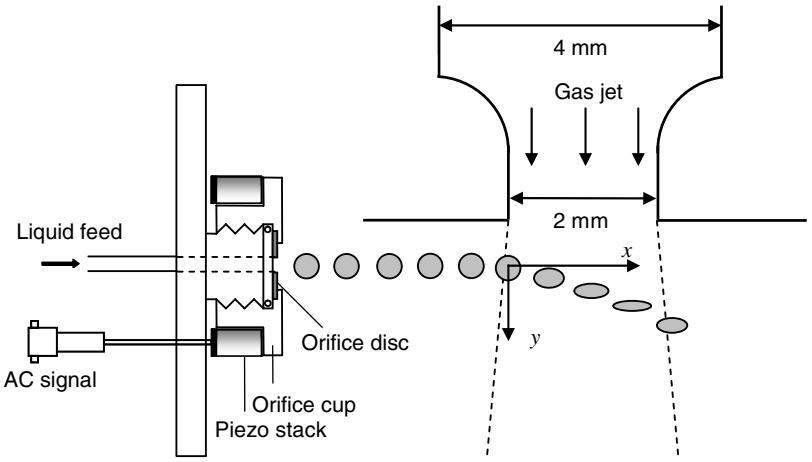

Fig. 1. Schematic diagram of droplet generator and gas nozzle.

In order to minimize the boundary-layer effects on the exiting gas jet, the gas nozzle with the rounded entrance with radius of 1 mm and exit diameter of 2 mm was used. Because the rounded passage feature of nozzle ensures that the thickness of the shear layer penetrated by the drops at the edge of jet is as thin as possible.

A droplet visualization system, as illustrated in Fig. 2, obtained the microscopic and macroscopic images. Microscopic images showing the breakup regime were captured by use of a spark lamp and a long distance microscope (QM-100, Questar). Alternatively, in the case of macroscopic images for analyzing the droplet distributions after breakup, a Nd:YAG laser and a CCD camera were used. The microscopic and macroscopic images utilized the shadowgraph and laser sheet methods, respectively. The delay generator (Berkeley Nucleonics Corp., Model 555) synchronized the flash lamp or Nd:YAG laser with the exposure of the CCD camera.

2.1.2. Phase Doppler particle analyzer system

The two-dimensional phase Doppler particle analyzer system analyzed the effect of the breakup regime on the size and velocity distributions. As shown in Fig. 3, the PDPA system consisted of an Ar-ion laser, transmitter, receiver, and Doppler signal analyzer. Since measuring size and velocity under conditions of high relative velocity is difficult, the power of the Ar-ion laser was controlled to 1.0 W. In addition, using the beam expander for the transmitter, the velocity measuring range of the PDPA system was extended from −292 m/s to 292 m/s. The sub-range of diameter i.e., the effective range of PDPA signal analyzer, was from 4 μm to

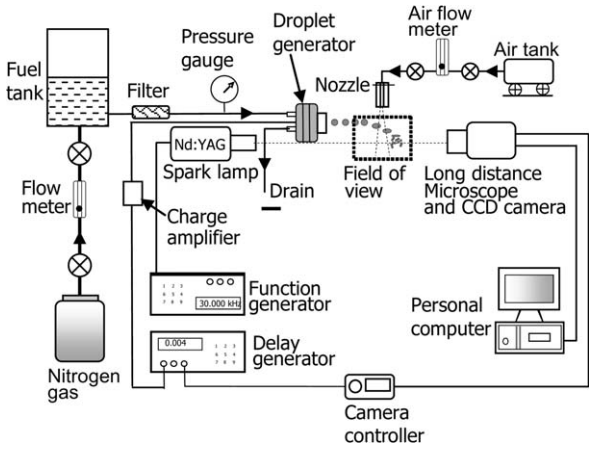

Fig. 2. Droplet visualization system.

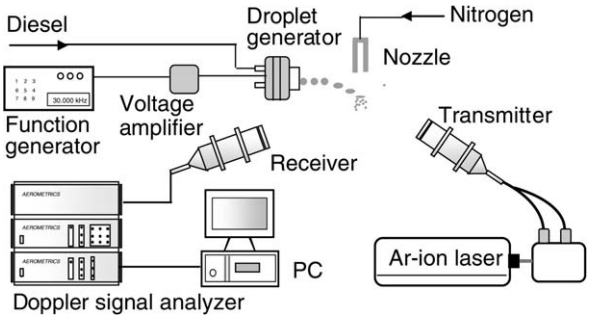

Fig. 3. Phase Doppler particle analyzer system.

200 μm, with consideration that theoretical size of a droplet produced by the droplet generator was 189 μm. For the measurement of droplet size and the velocity, the 20,000 droplets were collected and averaged at each measuring points.

2.2. Experimental procedure

The mono-dispersed droplets were generated using a vibrating orifice droplet generator. The generated droplets then disintegrated after exposure to the flow stream made by the gas jet injected through the nozzle. The velocity of the gas jet changed as a function of the mass flow rate of gas. In addition, the pressure difference between the droplet generator and ambient gas was set at a constant 0.1 MPa of gauge pressure. The inner diameter of the nozzle was 2 mm and the distance between the nozzle exit and the passage of the mono-dispersed droplet was set to a constant 1.5 mm.

The droplet size generated by the piezo stack droplet generator could be estimated by

$$D = \left(\frac{6\dot{Q}}{\pi f_{\text{opt}}}\right)^{1/3}. \tag{2}$$

In the above equation, D is the droplet diameter produced by the droplet generator of Fig. 2, and the optimal frequency (f_{opt}) could be determined by Eq. (1). In this experiment, the diameter of the orifice nozzle of the droplet generator (D_{n}) was set to 100 μm; therefore, the droplet size calculated by Eq. (2) yields 189 μm regardless of the flow rate.

The measurement points of the PDPA system were determined based on the macroscopic image shown in Fig. 4. The PDPA experiments were performed for three different cases of breakup regimes: bag, stretching and thinning, and catastrophic. As can be seen in Fig. 4, the measurement points exit at intervals of 2 mm in both axial and radial directions within the range in which the breakups actively occur. Additionally, the origins of the Z and R coordinates were the passage of the mono-dispersed droplet and the center of gas jet nozzle, respectively, as shown in Fig. 4(a).

The Weber number is an important factor in studying the breakup characteristics of droplets because it indicates the potential of the droplet breakup. In order to investigate the correlation between Weber numbers and breakup characteristics, the Weber (We) number was defined as follows:

$$We = \frac{\rho_{\text{G}} U^2 D}{\sigma_{\text{L}}}, \tag{3}$$

where, U and D represent the relative velocity between the droplet and ambient gas and the diameter of the droplet, respectively. The ambient gas density and the surface tension of liquid were represented by ρ_{G} and σ_{L}, respectively.

At the first breakup stage, the droplet deformed without disintegration due to the external force. In this regime, the deformation of the droplet is an important factor in analyzing the breakup mechanism. Therefore, in this study, the droplet deformation rate was quantitatively defined as shown in Fig. 5. The droplet deformation rate (ε) was defined as

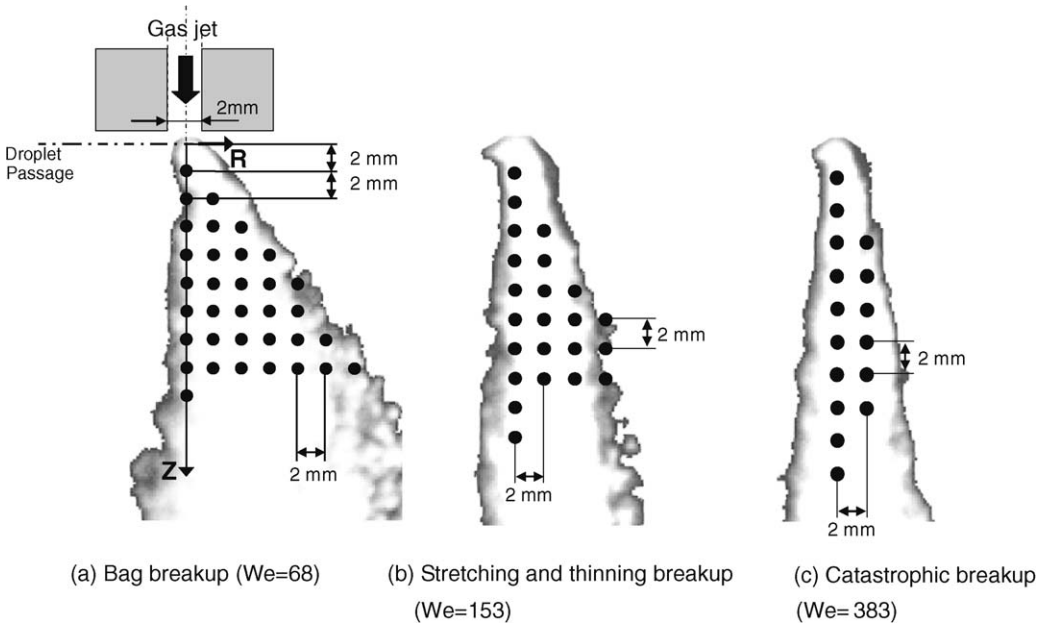

Fig. 4. Measurement points of the PDPA experiment according to the breakup regimes.

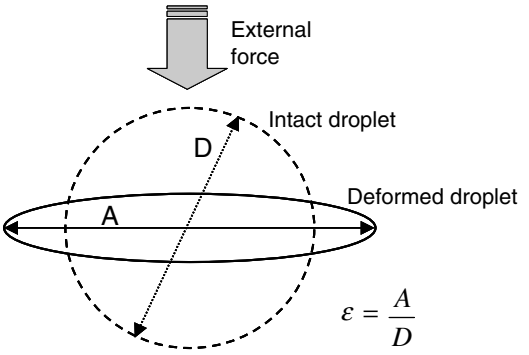

Fig. 5. Definition of the droplet deformation rate.

$$\varepsilon = \frac{A}{D}, \tag{4}$$

where A is the major axis of the deformed droplet, and D is the droplet diameter of an intact droplet.

The physical properties of the test diesel were: 831 kg/m^3 of density, 0.026 kg/s^2 of surface tension and 0.00223 kg/m^3 of viscosity. The detailed test conditions are listed in Table 1.

Table 1
Test conditions

Test fuel	Diesel
Applied frequency to droplet generator (kHz)	25–40
Weber number for visualization	2.4–664
Weber number for PDPA experiment	68, 153, 383
Nozzle orifice diameter (m)	100
Ambient pressure (MPa)	0.1
Ambient temperature (K)	293

3. Results and discussions

In order to investigate the atomization characteristics of mono-dispersed droplets in relation to the breakup regime, a piezoelectric droplet generator was used to produce the mono-dispersed droplets. Measurement of the size and standard variation from the PDPA system verified the produced droplets. Additionally, the effect of the Weber number on the droplet deformation rate was studied in the first breakup stage. In the second breakup stage, such as the bag, stretching and thinning, and catastrophic breakup regimes, the size and velocity distributions were measured using the PDPA system along with the macroscopic and microscopic visualizations.

3.1. Production of the mono-dispersed droplets

The properties of disintegrated droplets are highly dependent on the produced spherical droplets; therefore, the quality of the produced mono-dispersed particle from the droplet generator is important when studying the breakup characteristics of droplets. Prior to investigation of the breakup characteristics, the effect of the frequency applied to the droplet generator on the size and velocity distributions was studied. The measured diesel flow rate of the droplet generator nozzle orifice was 97.2 mg/s. Taking into account the orifice nozzle diameter of 100 μm, the theoretical optimal frequency could be calculated from Eq. (1) and was 33 kHz.

Fig. 6 shows the measurement results of droplet distribution and mean droplet size from the droplet generator. At an applied frequency of 33 kHz, which was the optimal frequency calculated from Eq. (1), the droplet size and the distances between droplets were exceptionally uniform without the generation of baby droplets. The AMD and SMD of the droplet were 184 μm, which was slightly smaller than the theoretical droplet size calculated from Eq. (2).

The effects of the applied frequency on the droplet size and velocity distributions were analyzed quantitatively, as shown in Fig. 7. At a frequency lower than 30 kHz, the mean diameter increased and the standard deviation decreased with the increase of the applied frequency, which indicates that the portion of the baby droplet decreased. At an applied frequency of 30 kHz, the standard deviation suddenly decreased because the baby droplets disappeared. After the optimal frequency, the mean size of a droplet decreased with an increase in the applied frequency, whereas the uniformity of produced droplets was constant.

As shown in Fig. 8, the velocities of the produced droplets were almost constant at a value of 13.4 m/s. This meant that the droplet velocity injected from the nozzle exit was influenced by the flow rate of liquid fuel and nozzle configuration, not the applied frequency.

3.2. Droplet deformation characteristics at the first breakup regime

Hwang et al. (1996) and Lee and Reitz (2001) presented the result that the droplets deform without breakup at the first breakup regime. Droplets experience deformation in their shape without disintegration due to the

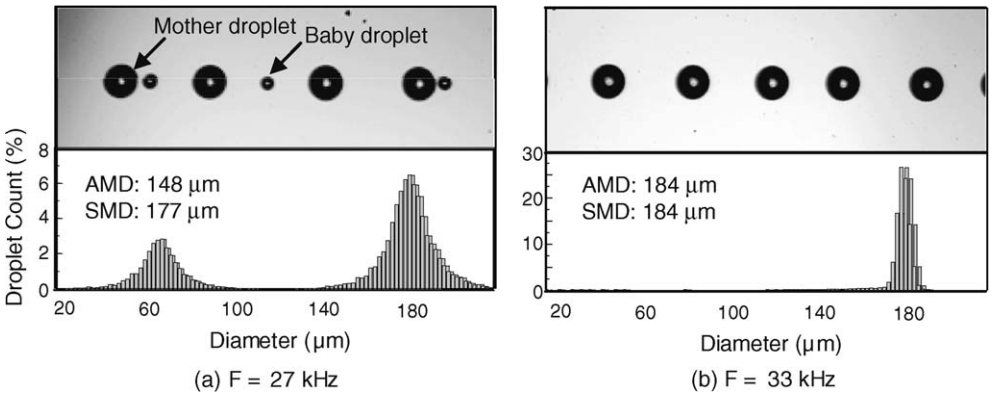

Fig. 6. Effect of the applied frequency on the production of droplets.

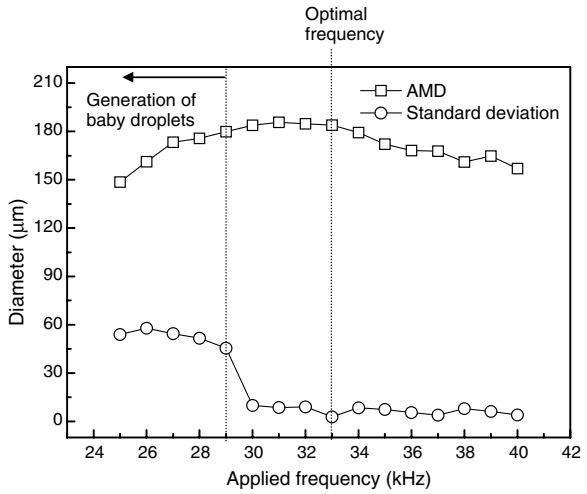

Fig. 7. Effect of the applied frequency on the droplet size and standard deviation.

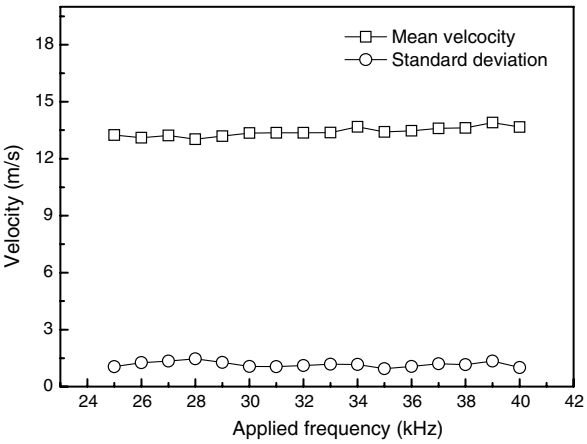

Fig. 8. Effect of the applied frequency on the droplet velocity and standard deviation.

external force during the process of the first break regime. After the droplet enters the gas flow field, the distribution of aerodynamic pressure around the droplet flattens it, as shown in the deformation images of Fig. 9.

Fig. 9 also illustrates the effect of the Weber number on the deformation rate, defined by Eq. (4). In this figure, the deformation rate increases as time increases until 100 μs subsequently, it decreases. The droplet flattened due to the external force until the external force was higher than the restoring force. However, the restoring force became higher as the deformation rate increased. In the range where the restoring force was higher than the external force, the droplet started to restore. Therefore, the deformation rate decreased after 100 μs.

3.3. Atomization characteristics of the droplets at the second breakup stage

As the Weber number increased from the first breakup stage, the droplets disintegrated as shown in Fig. 10. In this figure, in accordance to the increase of the Weber number, the breakup regime transitioned to the bag, stretching and thinning, and catastrophic breakup regimes, sequentially. The disintegration mechanisms of mono-dispersed droplets were different in relation to the breakup regimes. Because of this, an investigation

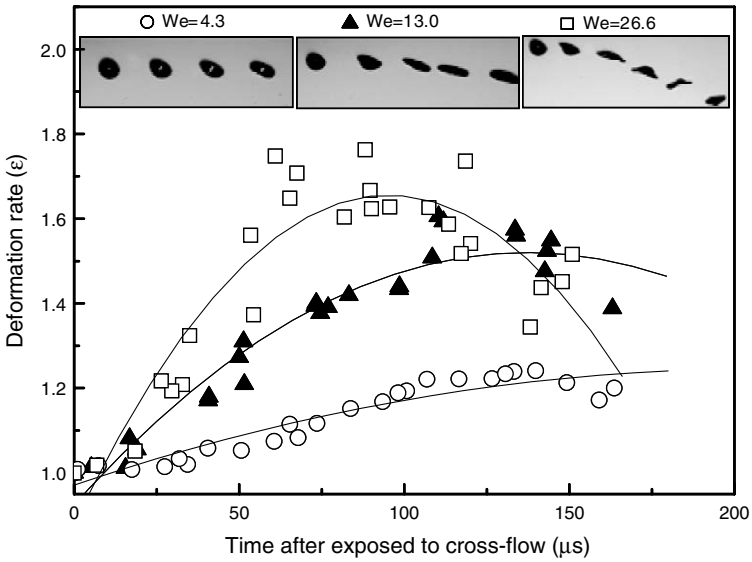

Fig. 9. Effect of Weber number on deformation of droplet at the first breakup stage.

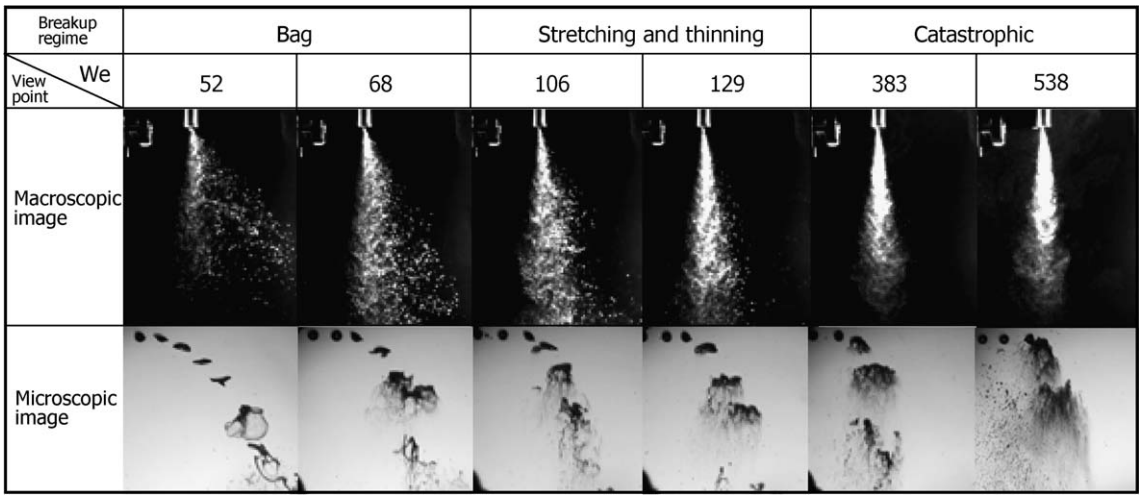

Fig. 10. Macroscopic and microscopic images according to Weber number.

was done on the breakup mechanisms and atomization characteristics in accordance to the breakup regimes by analyzing the microscopic and macroscopic images and the size and velocity distributions.

3.3.1. Bag breakup regime

When the Weber number was slightly higher than the critical value of the first breakup stage, a thin hollow bag, originating at the front stagnation point, started to form. As time elapsed in the gas flow, the bag grew and burst; thus, forming a number of small droplets as shown in the microscopic image of Fig. 11. The microscopic image also shows that the small droplets were detached from the large droplets during the burst process. The small droplets moved downward in correspondence to the ambient gas flow direction. Alternatively, the large droplets went further in the radial direction as compared to the small droplets. The loss of momentum explains this separation of small and larger droplets. The small droplets, detached from the large droplet, had

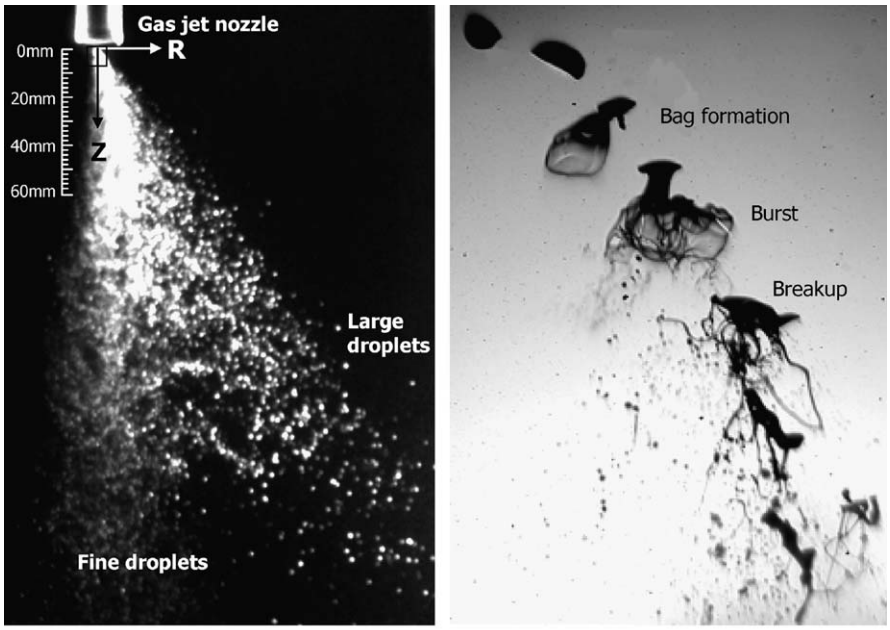

Fig. 11. Disintegration of droplets at bag breakup regime ($We = 68$).

a lower momentum than the large droplets. Therefore, the radial momentum of the small droplet rapidly decreased as shown in the SMD contour and velocity field of Fig. 12. Concurrently, the downstream gas flow increased the axial momentum of the droplet. Therefore, a cloud of fine droplets formed in the downstream region. In contrast,, the large droplets had a higher radial momentum than the small droplets. As a result, the small and large droplets had separate directions as shown in the macroscopic images of Fig. 11.

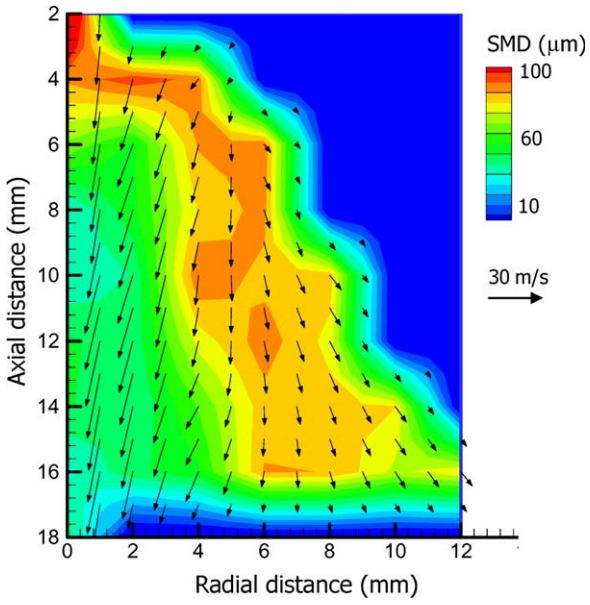

Fig. 12. Size and velocity distributions at bag breakup regime ($We = 68$).

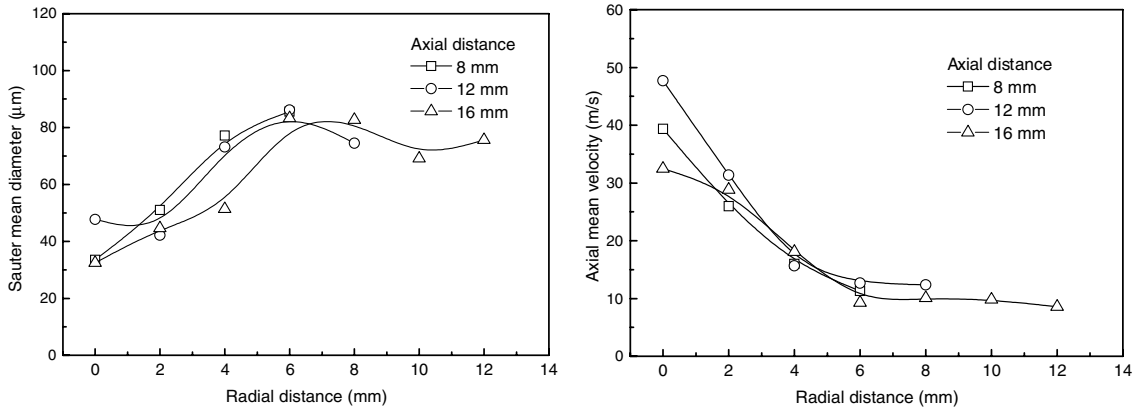

(a) Sauter mean diameter (b) Axial mean velocity

Fig. 13. Size and velocity distributions according to the radial distance at bag breakup regime.

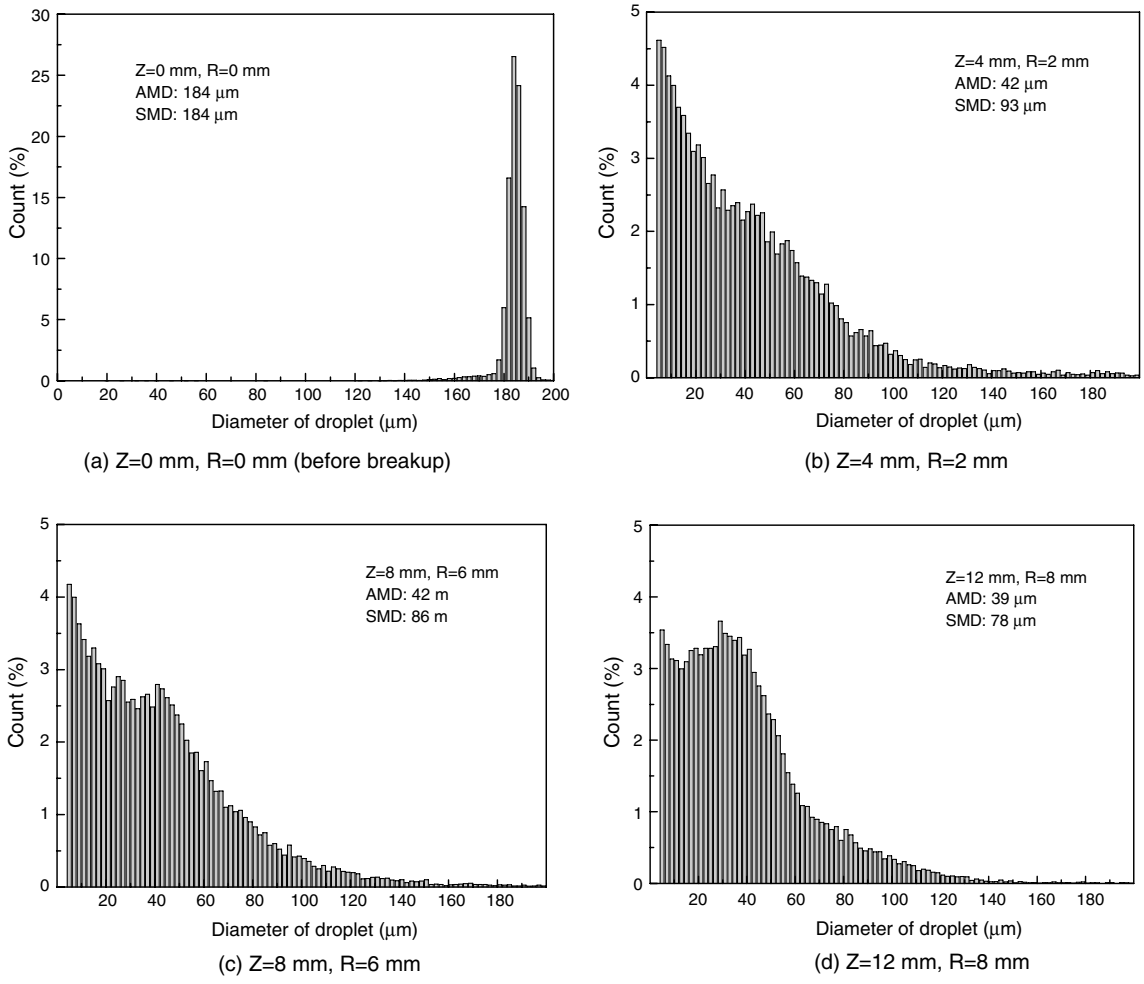

(a) Z=0 mm, R=0 mm (before breakup) (b) Z=4 mm, R=2 mm

(c) Z=8 mm, R=6 mm (d) Z=12 mm, R=8 mm

Fig. 14. Droplet size distributions at the main stream of droplets.

Fig. 12 illustrates the distributions of the SMD and velocity when the Weber number was 68. To reproduce this result, the measurement results were interpolated from the phase Doppler particle analyzer system. This figure shows that the SMD distribution was relatively high in the passage of large droplets, and low in the passage of small droplets. Additionally, Fig. 12 shows the high velocity region in accordance to the axis of the gas jet nozzle.

Fig. 13 shows the size and velocity distributions according to the radial distance at the bag breakup regime. As shown in Fig. 13, the SMD was higher in the region where the large droplets passed through; the SMD of large droplets was approximately 80 μm. Alternatively, in the passage of small droplets, the SMD was from 30 μm to 50 μm, which was smaller than the outer region. In the case of axial mean velocity, the droplets near the axis of the nozzle had a higher velocity and the axial mean velocity decreased as the measurement points moved outward.

In order to investigate the atomization process of large droplets at the bag breakup regime, the droplet size distributions were analyzed according to the main stream of the breakup as shown in Fig. 14. Before breakup, the initial droplet size was 184 μm. At a distance of 4 mm downstream the droplets were disintegrated by the bag breakup and the SMD was reduced to 93 μm, which was half of the intact droplet. Fig. 14(d) shows that the droplet counts from 40 μm to 60 μm increased as the measurement point moved downstream, as compared to Fig. 14. Simultaneously, droplet counts over 120 μm decreased. Based on these results, the conclusion was that droplets larger than 120 μm disintegrated into the smaller droplets with sizes from 40 μm to 60 μm as they moved downstream.

3.3.2. Stretching and thinning breakup regime

At the stretching and thinning breakup regime, droplets disintegrated at their edge because a suction stress toward the flow direction was generated at the surface of the droplet. In this regime, a shearing action due to the high-speed gas flow on the droplet caused the deformation of the droplet and the separation of the droplet surface.

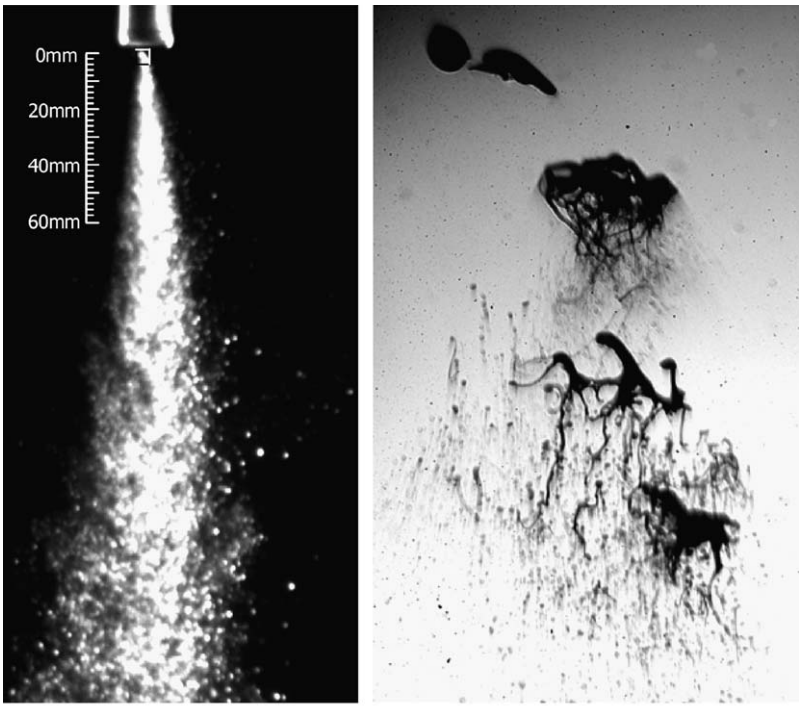

Fig. 15. Disintegration of droplets at stretching and thinning breakup regime ($We = 153$).

Fig. 15 shows the microscopic and macroscopic images of droplet disintegration and the droplet size and velocity distributions at the stretching and thinning breakup regime. In the macroscopic image, the droplets moved downstream after breakup, similar to a single spray, which was quite different from the case of the bag breakup regime. This phenomenon could be explained by a breakup duration that was short enough to lose the radial momentum of the droplet in this breakup regime. The illustration of droplet size and velocity distributions in Fig. 16 shows that the SMD distribution was higher near the nozzle and decreased as the axial distance increased.

For an axial distance at 153 of the Weber number, the size and velocity distributions were as illustrated in Fig. 17. In this figure, it can be seen that the SMD decreased with an axial distance above 10 mm. However, the AMD was nearly constant beyond 4 mm. This indicated that the breakup of droplets actively occurred above 4 mm and that relatively larger droplets were disintegrated from 4 mm to 10 mm. At a distance of 10 mm downstream, the droplet breakup process was almost completed. Additionally, the axial mean velocity increased with the increase of axial distance due to the gas jet flow field.

3.3.3. Catastrophic breakup regime

As the Weber number further increased from the stretching and thinning breakup regime, the breakup mechanism transitioned to the catastrophic breakup regime, as shown in Fig. 18. In this breakup regime, the breakup of the droplet occurred suddenly due to the wave instability on the droplet surface. Lee and Reitz (2001) presented that the possible wave instabilities at the catastrophic breakup regime can be classified into Kelvin–Helmholtz (KH) and Rayleigh–Taylor (RT) wave instabilities, and also showed that shear stress and acceleration on a droplet surface generate KH and RT waves, respectively. Therefore, in the case of a cross-flow gas stream, the dominant wave instability was RT, as illustrated in the microscopic image of Fig. 18. The macroscopic image of Fig. 18(a) shows that the disintegrated droplets moved downstream in a manner similar to the injected fuel spray through the injector. Fig. 19 shows the direction of droplets toward the axis of the gas jet nozzle.

Fig. 20 shows the size and velocity distributions according to the axial distance at the catastrophic breakup regime. In the case of the mean diameter, the AMD stayed practically constant while the SMD gradually decreased. As illustrated in the SMD and AMD distribution in Fig. 20, the SMD of droplets shows the rapid

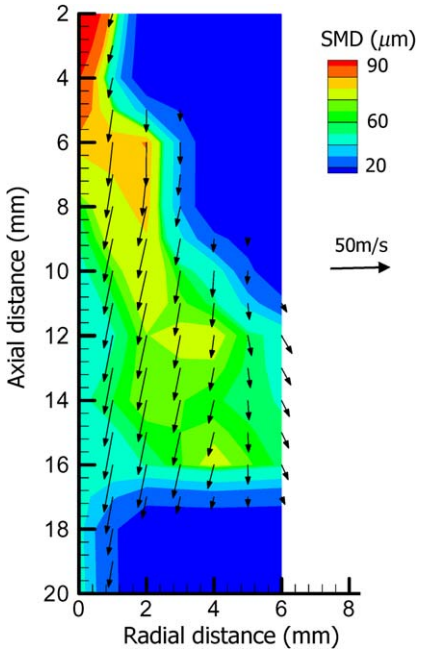

Fig. 16. Droplet size and velocity distribution at stretching and thinning breakup regime ($We = 153$).

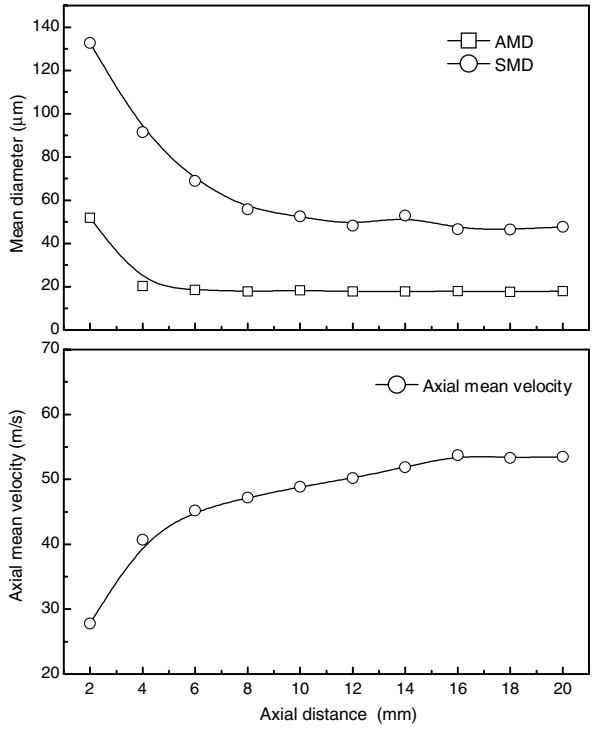

Fig. 17. Size and velocity distributions according to the axial distance ($We = 153$).

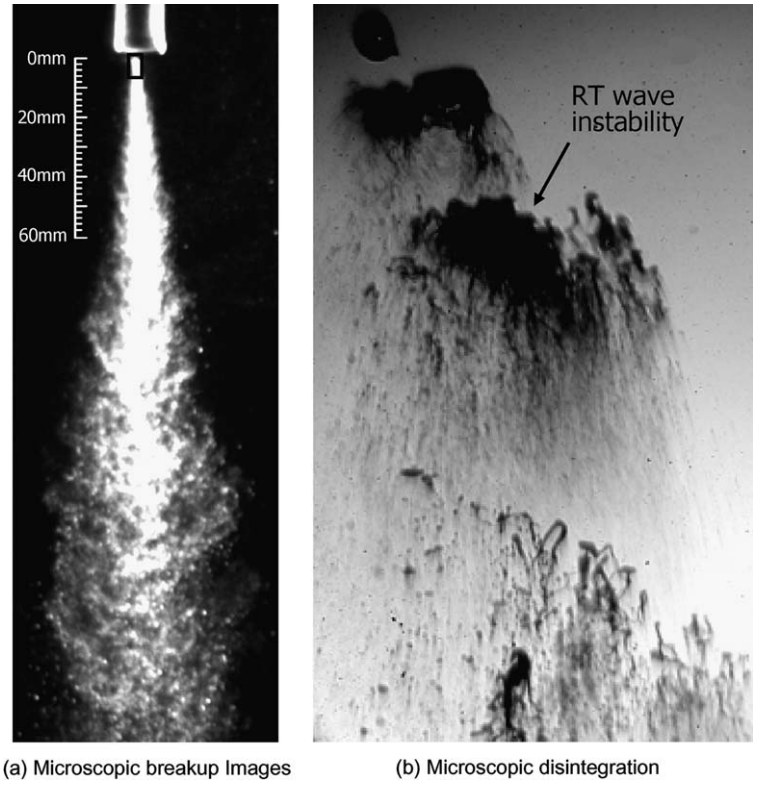

Fig. 18. Disintegration of droplets at catastrophic breakup regime ($We = 383$).

decrease with the increase of axial distance from the nozzle exit to vicinity of 4 mm. This demonstrates that the somewhat large droplet is being on the active catastrophic breakup above 4 mm of axial distance. But, in the

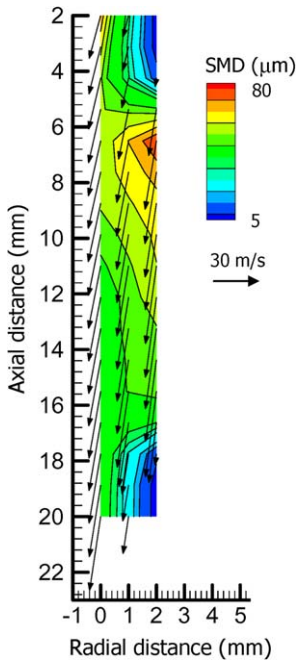

Fig. 19. Droplet size and velocity distributions at catastrophic breakup regime ($We = 383$).

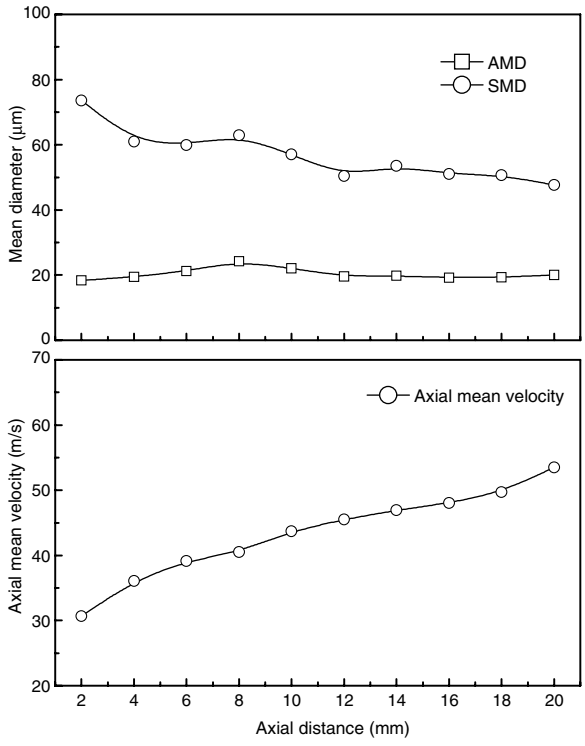

Fig. 20. Size and velocity distributions according to the axial distance ($We = 383$).

lower region beyond 4 mm, there is no more active breakup. Hence, it is concluded that the breakup process is almost completed above 4 mm of axial distance.

4. Conclusions

This study carried out experiments on the effect of a breakup regime on the atomization characteristics of mono-dispersed droplets. In order to generate mono-dispersed droplets with high uniformity, the characteristics of the produced droplets were investigated in accordance to the frequency applied to the piezoelectric droplet generator. The atomization characteristics were analyzed based on the microscopic and macroscopic images. In addition, the size and velocity distributions were obtained from the results of the droplet particle analyzer system. The conclusions of this study can be summarized as follows:

(1) At the first breakup stage, the deformation rate of a droplet increased with elapsed time. It then decreased because the restoring force became higher than the external force. Additionally, the deformation rate rapidly increased as the Weber number increased at the initial stage of deformation.
(2) The small droplets separated from the large droplets and moved downward because they rapidly lost radial momentum at the bag breakup regime. Alternatively, large droplets moved further in the radial direction as compared to the smaller droplets. Therefore, the droplets were classified into two groups; small and large droplets in the bag breakup regime.
(3) At stretching and thinning breakup, a cloud of droplets similar to a fuel spray was formed because the breakup duration was very short and radial momentum was extinguished rapidly in comparison to the bag breakup regime. The mean droplet size decreased to a certain distance and remained nearly constant as the axial distance increased. Similar characteristics were observed at the catastrophic breakup regime. However, the active atomization region of the catastrophic break regime was closer to the gas jet nozzle than that of the stretching and thinning breakup regime.

Acknowledgement

This work is financially supported by the Ministry of Education and Human Resources Development (MOE), the Ministry of Commerce, Industry and Energy (MOCIE) and the Ministry of Labor (MOLAB) through the fostering project of Lab of Excellency.

References

Baik, S., Blanchard, J.P., Corradini, M.L., 2003. Development of micro-diesel injector nozzles via MEMS technology and effect on spray characteristics. Atomization Sprays 13, 443–474.

Hountalas, D.T., Kouremenos, D.A., Mavropoulos, G.C., Binder, K.B., Schwarz, V., 2004. Multi-zone combustion modeling as a tool for DI diesel engine development-application for the effect of injection pressure, SAE paper 2004-01-0115.

Hsiang, L.P., Faeth, G.M., 1992. Near limit drop deformation and secondary breakup. Int. J. Multiphase Flow 19, 635–652.

Hwang, S.S., Liu, Z., Reitz, R.D., 1996. Breakup mechanisms and drag coefficients of high speed vaporizing liquid drops. Atomization Sprays 6, 353–376.

Kim, Y.D., Lee, S.Y., 2002. Application of Hough transform to image processing of heavily overlapped particles with spherical shapes. Atomization Sprays 12, 451–461.

Koh, K.U., Kim, J.Y., Lee, S.Y., 2001. Determination of in-focus criteria and depth field in image processing of spray particles. Atomization Sprays 11, 317–333.

Krzeczkowski, S.A., 1980. Measurement of liquid droplet disintegration mechanisms. Int. J. Multiphase Flow 6, 227–239.

Lee, C.S., Park, S.W., 2002. An experimental and numerical study on fuel atomization characteristics of high-pressure diesel injection sprays. Fuel 81, 2417–2423.

Lee, C.S., Reitz, R.D., 2001. Effect of liquid properties on the breakup mechanism of high-speed liquid drops. Atomization Sprays 11, 1–19.

Lee, K., Reitz, R.D., 2004. Investigation of spray characteristics from a low-pressure common rail injector for use in a homogeneous charge compression ignition engine. Meas. Sci. Technol. 15, 509–519.

Lee, C.S., Park, S.W., Kwon, S.I., 2005. An experimental study on the atomization and combustion characteristics of biodiesel-blended fuels. Energy Fuels 19, 2201–2208.

Liu, Z., Reitz, R.D., 1997. An analysis of the distortion and breakup mechanisms of high speed liquid drops. Int. J. Multiphase Flow 23, 631–650.

Park, S.W., Lee, C.S., 2003. Macroscopic structure and atomization characteristics of high-speed diesel spray. Int. J. Automotive Technol. 4, 157–164.

Park, S.W., Kim, H.J., Lee, C.S., 2003. Investigation of atomization characteristic and prediction accuracy of hybrid models for high-speed diesel fuel sprays, SAE paper 2003-01-1045.

Payri, F., Payri, B.R., Salvador, F.J., 2004. The influence of cavitation on the internal flow and the spray characteristics in diesel injection nozzles. Fuel 83, 419–431.

Schunemann, E., Fedrow, S., Leipertz, A., 1998. Droplet size and velocity measurements for the characterization of a DI-diesel spray impinging on a flat wall, SAE paper 982345.